

Biophysical and yield information for precision farming from near-real-time and historical Landsat TM images

P. S. THENKABAIL

Center for Earth Observation (CEO), Department of Geology and Geophysics,
Kline Geology Laboratory, PO Box 208109, 210 Whitney Avenue,
Yale University, New Haven, CT 06520-8109, USA;
e-mail: prasad.thenkabil@yale.edu

(Received 8 June 2001; in final form 9 April 2002)

Abstract. The main goal of this study was to quantify within and between field variability in mapping agricultural crop types, their biophysical characteristics, and yield for precision-farming applications using near-real-time and historical (archival) Landsat Thematic Mapper (TM) images. Data for six crops (wheat, barley, chickpea, lentil, vetch and cumin) were gathered from a representative benchmark study area in the semi-arid environment of the world. Spectro-biophysical and yield models were established for each crop using a near-real-time TM image of 6 April 1998 acquired to coincide with an extensive ground data collection campaign. The models developed using this near-real-time acquisition were then used to extrapolate and quantify characteristics in the historical Landsat TM images of 5 April 1986 and 4 May 1988 acquired for the same area with limited ground data, thus adding scientific and commercial value to archival TM images. A farm-by-farm (or pixel-by-pixel) within and between field variability in agricultural land cover, biophysical quantities [e.g. biomass and Leaf Area Index (LAI)] and yield was established and illustrated. For the near-real-time image of 1998: (a) quantitative biophysical characteristics such as LAI and biomass were mapped at 81% overall accuracy ($K_{\text{nat}} = 0.76$) or higher; (b) within field variability (commission errors) was mapped with an accuracy between 74–100%; and (c) between field variability (omission errors) was mapped with an accuracy between 76–100%. Temporal variability in biomass and LAI were mapped for the study area and highlighted for individual farms. Significant relationships existed between grain yields measured using field-based combine-mounted sensors and Landsat TM derived indices. The results demonstrate the ability of using near-real-time and historical Landsat TM images for obtaining quantitative biophysical and yield information that highlight within and between field variability, which is of critical importance in precision-farming applications.

1. Introduction and background

The use of satellite sensor derived data to quantitatively and qualitatively assess within and between field variability of agricultural crops is increasingly becoming the single most important information source for precision farming. Remote sensing applications for precision farming have entered a new era, ushered in with successful launches of hyperspatial sensors such as IKONOS, and hyperspectral sensors such as Hyperion onboard National Aeronautics and Space Administration (NASA)'s

Earth Observing-1 (EO-1). These newer satellite sensor systems dramatically increase spatial, spectral, radiometric and temporal frequencies (table 1) and thus make them appealing to precision-agriculture applications. Data from Landsat and Landsat-type systems have significantly lower numbers of data points per ha (table 2) when compared to systems such as IKONOS (table 1). However, Landsat and the Landsat-type sensors such as the Système Probatoire de l'Observation de la Terre (SPOT), and the Indian Remote Sensing (IRS) satellites are of equal importance in precision farming due to their large synoptic view, substantial historical archive over the past three decades, additional spectral bands (e.g. in mid-infrared and thermal infrared

Table 1. Characteristics of data gathered from very high spatial resolution sensors suitable for precision farming.

Satellite/sensor	Spatial resolution (m)	Spectral resolution (no. of bands)	Data points or pixels per ha
IKONOS 2 SpaceImaging	1 (P), 4 (M)	4	10 000, 625
QUICKBIRD EarthWatch	0.82 (P), 4 (M)	4	14 872, 625
Orbview-4 Orbital imaging	1 and 2 (P) 4 (M), 8 (H)	4 + hyperspectral	10 000, 2500 625, 156
EROS A Imagesat	1.82 (P)	1	3020

M = multispectral; P = panchromatic, H = hyperspectral.
EROS = Earth Resources Operation System.

Table 2. Characteristics of data gathered from satellite sensors of different eras suitable for precision farming.

Satellite/sensor	Spatial resolution (m)	Spectral bands (no. of bands)	Data points or pixels per ha
Earth Observing-1 Hyperion	30	220 (400–2500 nm)	11.1
ALI	10 (P), 30 (M)	1, 9	100, 11.1
Terra: EOS ASTER	15, 30, 90 (VNIR, SWIR, TIR)	4, 6, 5	44.4, 11.1, 1.26
MODIS	250–1000	36	0.16, 0.01
Landsat-7 TM	15 (P), 30 (M)	7	44.4, 11.1
IRS-1C LISS	5 (P), 23.5 (M)	3	400, 18.1
IRS-1D LISS	5 (P), 23.5 (M)	3	400, 18.1
SPOT-1, 2, 3, 4 HRV	10 (P), 20 (P)	4	100, 25
Landsat-4, 5 TM	30 (M)	7	11.1
Landsat-1, 2, 3 MSS	56 × 79	4	2.26

M = multispectral, P = panchromatic.

ALI = Advanced Land Imager; EOS = Earth Observing System; LISS = Linear Imaging Self-scanning Sensor; MSS = Multi-Spectral Scanner.

that are absent in IKONOS), reasonably high spatial resolution of 30 m or better, and well understood spectro-biophysical relationships over the years. The data from older and newer generation sensors are supplemented by advances in ground-based combine-mounted sensors for real-time yield assessments, digital cameras, imaging spectrometers, Geographical Information System (GIS) and Global Positioning System (GPS) technology, sophistication in computer hardware and software, and internet delivery of data (Fritz 1996). All of this has stimulated the packaging of a complex suite of technologies to provide agricultural crop information in near-real time to facilitate precision farming and delivered to farmers, farm managers, agricultural extension officers and decision makers.

Site-specific information of agricultural crop conditions is essential for precision farming. Precision crop management requires spatial information on crop condition, biomass and yield productivity at different stages of growth within and between seasons. Remote sensing provides consistent within and between field spatial variability across seasons in biophysical characteristics and yield that can be related to a crop model, making the decision-making approach feasible for precision-farming applications (Jones and Barnes 2000). For example, the multispectral and hyperspectral data can be converted into quantitative and/or qualitative maps or information showing pixel-by-pixel variability for direct application in precision farming. Quantitatively spectral data are converted into biophysical quantities like Leaf Area Index (LAI) and biomass and integrated into crop growth models (Moran *et al.* 1995, Johannsen *et al.* 1998). Qualitatively, variability is mapped in terms of magnitude such as high and low levels of pest and disease infestation, high and low levels of nitrogen deficiency, high and low stress levels of soil organic matter variability, within or across farms. Crop yield and growth parameters (LAI, biomass) mapped based on remotely sensed data enable fast, non-destructive and relatively cheap characterisation of crop status, provide input data for growth simulation models and allow for spatial extrapolation of results at regional levels (see Vaesen *et al.* 2001). The farmers and farm managers can use these maps directly or can incorporate information contained in them into crop models or decision support systems to enable site-specific micro management of farms. Usery *et al.* (1995) define precision farming as the application of a combination of advanced technologies to: (a) improve agricultural crop productivity and (b) reduce environmental pollution through quantitative and qualitative information of within field variability (or site-specific variability) caused by natural and manmade causes.

In modern agriculture, the need to balance production with environmental concerns and sustainability of the systems is of high importance and requires consistent, timely, repeatable information of the within and between field variability of the farm. Precision crop management (PCM) is known to increase net return per acre, increases the efficiency of agricultural inputs, reduces the risk of endangering the quality, and promotes increased management skills (Barnes *et al.* 1996, Moran *et al.* 1997). Crop yield is currently estimated overwhelmingly using weighing conveyor technology. Recent introduction of combine-mounted sensors requires farmers to handle one more bit of technology, which is not appreciated horizontally across the farming community. Further, it also introduces inconsistencies in setting up and recording data from farmer to farmer. Effective, consistent and rapid assessments of yield estimates are possible using remotely sensed data, especially when such data are available in later stages of crop growth. This has become more reliable with data availability from newer hyperspatial sensors such as IKONOS and ASTER. The

in situ measurement of within and between field variability in agricultural crops or vegetation characteristics are resource intensive and are currently being phased out with the availability of cheaper and/or much more sophisticated spatial technologies that are widely proliferating and involve remote sensing, GIS and GPS. Quantification of infection is generally more efficient by the aforementioned imaging techniques than by visual assessment. Pre-harvest crop yields are best predicted using images late in the crop-growing season (see Moran *et al.* 1997). Remote sensing derived maps show pixel-by-pixel variability of yield within and between each farm field, highlighting the site-specific characteristics of the farm field. Thus, yield maps have been used directly for management of fertiliser application, water application, planting strategies, soil management, and in management of weeds, insects and diseases (Moran *et al.* 1997).

Given the increasing importance of remote sensing in precision farming, the need for well understood studies that map and highlight pixel-by-pixel and farm-by-farm variability in biophysical quantities and yield are required for various crops grown in a wide range of environments. The study will focus on using Landsat images for precision farming in order to identify, map, quantify and assess farm-by-farm (but spread across entire regions) spatial and temporal variability for maximising profits, to enable sustainable production and for protecting the environment. The key information requirements of precision farming are summarised by Moran *et al.* (1997) as: (a) seasonally stable conditions (e.g. soil maps, topography, grain yield maps), and (b) seasonally variable conditions (e.g. crop biophysical parameters, crop growth, phenology, crop disease, weed infestation, nutrient deficiencies, soil types or characteristics, and evapotranspiration rates). Based on this information, diagnosis of the cause of variability in crop growth and/or yield is determined and appropriate management strategies formulated. The focus of this paper will be on methods to determine and map seasonally variable conditions.

This study was conducted in a representative benchmark research area in the semi-arid environments of the world using a near-real-time Landsat Thematic Mapper (TM) image and two historical Landsat TM images of the same area (table 3(a)). Agricultural crop characteristics were quantified using a near-real-time TM image of 6 April 1998. Extensive fieldwork was conducted to correspond with the 1998 image acquisition. Spectro-biophysical and yield relationships were developed for six crops based on this data set. The relationships were used to extrapolate results to historical (archival) TM images of 1986 and 1988. The main goals of the study were: (1) to develop methods and to illustrate and map pixel-by-pixel and farm-by-farm within and between field variability in biophysical characteristics and yield of six agricultural crops using near-real-time image of 1998; and (2) to extrapolate the spectro-biophysical and yield relationships developed using 1998 image to historical images of 1986 and 1988. This will help to understand the temporal changes in quantitative biophysical and yield characteristics over decades, adding immense value to archival (historical) data.

2. Study area

The study area (figure 1) is representative of the desert margins of the world and is located in the Syrian Arab Republic. Over a billion people live in the desert margins, and 50% of them depend on agriculture for a livelihood. The study region is characterized by a Mediterranean climate: hot and dry summers and cool and wet

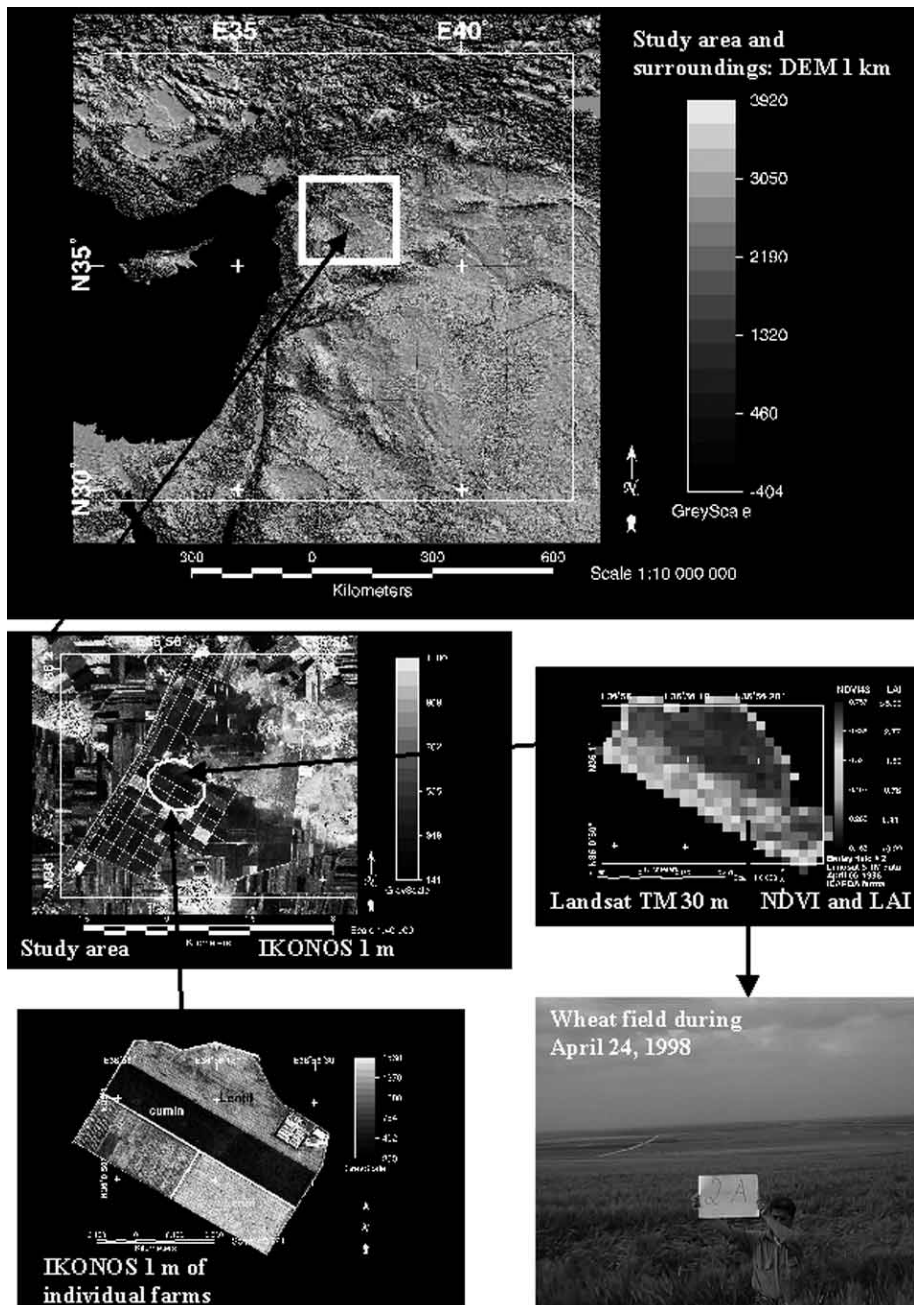


Figure 1. Benchmark study area location in the Syrian Arab Republic.

winters. The annual rainfall varies from 300–350 mm. This climate pattern occurs in several locations in the 30–40° latitude belts in both hemispheres. The largest single contiguous area experiencing this climate is in the Mediterranean basin covering parts of west Asia, north Africa and southern Europe. Many summer and winter crops in this climate are common, with similar growing seasons and management

Table 3(a). Radiometric and solar elevation calibration coefficients for the three Landsat TM images used in this study.

Acquisition date	Radiometric parameter units (W m ⁻² sr ⁻¹ μm ⁻¹)							Solar elevation (°)	Solar azimuth (°)
		TM1	TM2	TM3	TM4	TM5	TM7		
6 April 1998	alpha = gain	0.6340139	1.2581045	0.9668220	0.9105893	0.1253798	0.0670115	51.00	133.00
	beta = offset	-1.1242424	-1.8634146	-1.6089552	-1.6335938	-0.2543779	-0.1273810		
5 April 1986	alpha = gain	0.6024314	1.1750981	0.8057647	0.8145490	0.1080784	0.0569804	49.47	131.29
	beta = offset	-1.5200000	-2.8400000	-1.1700000	-1.5100000	-0.3700000	-0.1500000		
4 May 1988	alpha = gain	0.6024314	1.1750981	0.8057647	0.8145490	0.1080784	0.0569804	58.42	122.38
	beta = offset	-1.5200000	-2.8400000	-1.1700000	-1.5100000	-0.3700000	-0.1500000		

Table 3(b). Improved dark object atmospheric haze correction values using relative scattering model suggested by Chavez (1988, 1989).

	Atmosphere condition	Relative scattering model	TM1 Starting haze value (No.)	TM2 Haze value to deduct (No.)	TM3 Haze value to deduct (No.)	TM4 Haze value to deduct (No.)	TM5 Haze value to deduct (No.)	TM7 Haze value to deduct (No.)
6 April 1998	Very clear	$\lambda^{-4.0}$	50	10	6	0	0	0
5 April 1986	Very clear	$\lambda^{-4.0}$	72	18	15	5	1	0
4 May 1988	Very clear	$\lambda^{-4.0}$	78	23	18	9	1	0

Table 3(c). Radiometric and atmospheric normalization of multitemporal images using very dark and bright objects¹ (after Elvidge *et al.* 1995).

TM band	Intercept	Slope	R ²
5 April 1986 relative to 6 April 1998 ²			
TM1 of 1986=	-2.89821	0.794643	0.97
TM2	-2.02974	0.788104	0.99
TM3	-1.342	0.706559	0.99
TM4	-1.42027	0.810667	0.99
TM5	-1.25396	0.770791	0.99
TM7	-0.94333	0.746296	0.98
4 May 1988 relative to 6 April 1998 ²			
TM1 of 1988 image=	1.63053	0.690815	0.95
TM2	-2.27881	0.839604	0.99
TM3	-0.0971	0.683742	0.97
TM4	-0.24968	0.786546	0.97
TM5	-1.1686	0.697888	0.98
TM7	-1.35983	0.586608	0.95

¹Equations are based on plots reflectance in a dark object (deep water) and a bright object (concrete and high albedo soils).

² $Y = a + bx$, where x is the digital number for 1998.

practices. Most of the cultivation is rain fed during the winter and spring (mid-November to early May). Supplemental irrigation is carried out either through deep wells or from the canals from the reservoir built across the Euphrates River. The land use intensity is high with most of the arable land already used for agriculture. The specific focus of this study will be in a 3600 ha area where detailed ground measurements were made.

3. Materials and methods

3.1. Images used in the study

Three Landsat TM images (table 3(a)) were obtained to study rain fed crops of winter and spring season. The images were acquired to correspond with late vegetative or critical growing conditions of most crops (table 4). All images were rectified using ERMapperTM software based on the 22 ground control points collected during fieldwork using a GarminTM GPS. This resulted in a rms error of about zero.

3.2. Field measured agricultural crop characteristics

Ground data were collected from 205 locations (see the ground data point locations in figure 1). The data were collected for six major crops: barley (*Hordeum vulgare* L.; sample size 44), wheat (*Triticum aestivum* L. or *Triticum durum* Desf.; 64), lentil (*Lens esculenta* Moench. Or *Lens orientale* (Boiss.) Schmalh. Or *Lens culinaris* Medikus; 23), cumin (*Cuminum cyminum* L.; 17), chickpea (*Cicer arietinum* L.; 14) and vetch (*Vicia narbonensis* L.; 14). Data were gathered from the researcher-managed farms and farmer-managed farms. Researcher-managed farms are maintained by the International Center for Agriculture in the Dry Areas (ICARDA), south-west of Aleppo, Syria (small boxed area in the middle image in figure 1). Farmer-managed farms are spread over a much larger area of about 50 km × 50 km. Measurements were also taken from marginal lands (20) and fallow farms or top soils (nine).

Table 4. General characteristics of agricultural crops.

Crop type and (sample size)	Mean ground-measured crop variables ¹								Mean Landsat-5 TM bands ²					
	Wet biomass (kg m ⁻²) WBM	Dry biomass (m ² m ⁻²) DBM	Leaf area index (m ² m ⁻²) LSI	Plant height (mm) PLNTH	Canopy cover (%)	Crude protein (%)	Nitrogen (%)	Moisture (%)	TM1	TM2	TM3	TM4	TM5	TM7
Barley (44)	2.54	0.89	2.09	789	97	7.3	1.17	65	56.2	23.3	20.7	86.3	51.4	17.6
Chickpea (14)	1.41	0.30	1.59	365	69	18.8	3.01	79	60.9	28.5	37.0	63.7	74.6	34.6
Cumin (17)	0.82	0.19	0.60	190	48	19.6	3.13	77	61.6	29.2	43.4	53.9	81.6	44.0
Lentil (23)	2.49	0.79	2.64	345	90	16.8	2.68	68	59.9	27.4	28.9	82.5	71.5	28.7
Marginal (20)	0.90	0.38	N/A	236	68	9.5	1.52	58	65.1	31.1	32.3	87.6	86.5	33.8
Vetch (14)	3.22	0.33	2.94	381	88	19.8	3.17	90	59.5	27.1	28.8	83.9	73.4	29.9
Wheat (64)	3.28	0.83	3.21	776	97	10.4	1.66	75	56.1	22.9	22.4	84.9	55.0	19.9
Test of significance at 95% confidence level ³ : Agricultural crops that are significantly different from each other (e.g. ba-ch) in a TM band (e.g. TM1) are listed. At the end the total number of differences between two crops are listed.				ba-ch, ba-cu, ba-le, ba-ma, ch-ma, ch-wh, cu-ma, cu-wh, le-ma, le-wh, ma-ve, ma-wh, ve-wh	ba-ch, ba-cu, ba-le, ba-ma, ba-ve, ch-ma, ch-wh, cu-wh, le-ma, le-wh, ma-ve, ma-wh, ve-wh	ba-ch, ba-cu, ba-le, ba-ma, ba-ve, ch-cu, ch-le, ch-ma, ch-ve, cu-le, cu-ma, cu-ve, cu-wh, le-wh, ma-wh, ve-wh	ba-ch, ba-cu, ch-cu, ch-le, ch-ma, ch-ve, cu-ma, cu-ve, cu-wh	ba-ch, ba-cu, ba-le, ba-ma, ba-ve, ch-ma, ch-wh, cu-le, lu-wh, le-ma, le-wh, ma-ve ma-wh, ve-wh	ba-ch, ba-cu, ba-le, ba-ma, ba-ve, ch-cu bh-le, ch-wh, lu-le, cu-ma, cu-ve, cu-wh, le-ma, le-wh ma-wh, ve-wh	ba-ch, ba-cu, ba-le, ba-ma, ba-ve, ch-cu bh-le, ch-wh, lu-le, cu-ma, cu-ve, cu-wh, le-ma, le-wh ma-wh, ve-wh	ba-ch, ba-cu, ba-le, ba-ma, ba-ve, ch-cu bh-le, ch-wh, lu-le, cu-ma, cu-ve, cu-wh, le-ma, le-wh ma-wh, ve-wh	ba-ch, ba-cu, ba-le, ba-ma, ba-ve, ch-cu bh-le, ch-wh, lu-le, cu-ma, cu-ve, cu-wh, le-ma, le-wh ma-wh, ve-wh	ba-ch, ba-cu, ba-le, ba-ma, ba-ve, ch-cu bh-le, ch-wh, lu-le, cu-ma, cu-ve, cu-wh, le-ma, le-wh ma-wh, ve-wh	ba-ch, ba-cu, ba-le, ba-ma, ba-ve, ch-cu bh-le, ch-wh, lu-le, cu-ma, cu-ve, cu-wh, le-ma, le-wh ma-wh, ve-wh
The results indicate that TM3 has the highest number of cases of separating two crops spectrally, followed by TM7 and TM5.				Total = 13	Total = 13	Total = 17	Total = 11	Total = 14	Total = 16					

¹Ground truth data were gathered in April–May 1998.²Landsat-5 TM data are for 6 April 1998 image.³ba = barley, ch = chickpea, cu = cumin, le = lentil, ma = marginal lands, ve = vetch, wh = wheat.

Quantitative and qualitative ground data (table 4) were collected during April 1998 that corresponded with Landsat TM data acquisition. Plant characteristics obtained (table 4) included LAI, wet biomass (WBM), dry biomass (kg m^{-2}), plant height (PLNTH), canopy cover (%), crude protein (%), nitrogen (%), crop moisture (%) and growth stage (based on crop calendar). Details of the procedure for gathering these data are described in Thenkabail *et al.* (2002). Crop type and crop calendar data were available for all three years (1986, 1988 and 1998) for the researcher-managed farms of ICARDA. These were provided in terms of field maps. Researcher-managed farms constituted about 40% of all ground data. Of the 3600 ha of the focus study area, 980 ha were researcher-managed; farmers managed the rest. The average field size was about 5 ha.

3.3. Landsat TM derived agricultural crop characteristics

In order to develop spectro-biophysical and yield relationships, digital values were extracted from six non-thermal bands of the Landsat-5 TM data from: (a) the entire field; (b) a 3×3 pixel area within each field; and (c) three random pixels within each field. For the procedures to work the ground samples must adequately portray the conditions contributing to vegetation index response (Anderson *et al.* 1993). By averaging the vegetation index over a 9-pixel area, for example, a single ground sample had to capture the average condition of a region 8100 m^2 . A more desirable situation would be the comparison of the sample point to the vegetation index value obtained for a single pixel (900 m^2) (see Anderson *et al.* 1993). However, locating a precise pixel was difficult. Preliminary analysis showed that the 3-pixel procedure provided the better results. Hence a 3×3 pixel area (8100 m^2) within each field was selected. These pixels were selected by taking the GPS location of the sample site as the centre of 3×3 pixel. The mean digital numbers for six crops and marginal lands for the 1998 image are presented in table 4.

3.4. Atmospheric correction

Before extracting any information, atmospheric effects were normalised for three study images. Regression analysis as suggested by Elvidge *et al.* (1995) was attempted resulting in regression equations for each band (table 3(c)). However, this method suffered from great difficulty in determining a 'perfect' bright object over a decade-long duration. Alternatively, scene-based atmospheric scattering correction was done using the Chavez modified dark-object subtraction technique (Chavez 1988, 1989). In arid and semi-arid regions most atmospheric effects are due to scattering of light by gas molecules and aerosols. The Chavez technique is based on the theory that the degree of scattering is strongly wavelength-dependent: it affects blue wavelengths much more than red and infrared wavelengths. Hence the method is well suited for the study area, which is predominantly in a semi-arid region. Rayleigh relative scattering model of $\lambda^{-4.0}$ was used (table 3(b)) for the 1998 and 1986 images since they were 'very clear' images. For a 'clear' image of 1988, $\lambda^{-2.0}$ was used. The method involves selecting a starting haze value (SHV) by plotting and observing the histograms of band 1 where atmospheric effects are most pronounced (Milton 1994). The Chavez model then calculates haze affected band values for other bands (table 3(b)). The haze affected band values of each band are then deducted from the original band values. The theory here is that the digital numbers or reflectance over perfect 'dark objects' (e.g. unpolluted deep waterbodies) should remain unchanged from time period 1 to time period 2 if not for atmospheric effects.

3.5. Digital numbers to radiance

Digital numbers were converted to spectral radiance (Price 1987) using the equation:

$$R_i = \alpha_i \text{DN}_i + \beta_i \quad (1)$$

where R_i = spectral radiance in $\text{W m}^{-2} \text{sr}^{-1} \mu\text{m}^{-1}$; α_i = gain or slope in $\text{W m}^{-2} \text{sr}^{-1} \mu\text{m}^{-1}$ (table 3(a)); β_i = bias or intercept in $\text{W m}^{-2} \text{sr}^{-1} \mu\text{m}^{-1}$ (table 3(a)); DN_i = digital number of each pixel or mean of a number of pixels in TM bands where $i = 1-5$ and 7 (except thermal band 6). This normalised for sensor degradation and other changes in sensor data acquisition characteristics. Since multitemporal images of 1998, 1988 and 1986 were acquired it was essential to convert digital counts of each farm to radiance and then to at-satellite exoatmospheric reflectance (R_{exo}).

3.6. Radiance to at-satellite reflectance

Radiance values were converted to at-satellite exoatmospheric reflectance (ρ_p) using the equation:

$$\text{at-satellite or apparent reflectance } (\rho_p) = \frac{\pi R_i d^2}{\cos(\theta) F_0} \quad (2)$$

where the Earth–Sun distance is d (unitless), which varies between 0.96–1.04, can be obtained from nautical handbook (see Markham and Barker 1987), but is often assumed as 1, and the solar zenith angle is θ (which is 90° minus the Sun elevation or Sun angle when the scene was recorded as given in the image header file) (see table 1). For example, the solar elevation for the 5 April 1986 image was 49.47° (from Earth Observing Satellite (EOSAT) header file) and hence θ will be 40.53° . Solar flux or exoatmospheric irradiances (F_0) can be found in Neckel and Labs (1981 and 1984). F_0 ($\text{W m}^{-2} \text{sr}^{-1} \mu\text{m}^{-1}$) for TM bands were: TM1, 1946.48; TM2, 1812.63; TM3, 1545.95; TM4, 1046.7; TM5, 211.12; TM6, 1; and TM7, 76.91. This equation normalises measurements for solar elevation (table 3(a)), solar flux and Earth–Sun distance.

3.7. Spectro-biophysical relationships

To represent the relationship between the various vegetation indices, VI_j , and biophysical quantities, B_i , both linear and non-linear models need to be fitted based on the plot appearance and best-fit R^2 values. When nonlinearity existed, exponential, power or quadratic models were attempted. The equation forms were: (1) exponential, $B_i = ae^b(\text{VI}_j)$; (2) linear, $B_i = a + b(\text{VI}_j)$; (3) quadratic, $B_i = a(\text{VI}_j)^2 + b(\text{VI}_j) + c$; and (4) power, $B_i = a(\text{VI}_j)^b$; where a = slope, b = intercept of soil line (obtained by plotting red versus near-infrared (NIR) bands) and VI = vegetation index. The biophysical quantities were LAI, biomass, plant height and grain yield. Most of the best spectro-biophysical relationships were either nonlinear exponential or linear. On rare occasions, quadratic or power models provided slight increase in R^2 values, but these increases were generally insignificant. Hence only linear or nonlinear exponential relationships are reported in this paper.

3.8. Spatial mapping of quantitative biophysical relationships

First, well-understood spectro-biophysical and yield relationships were developed using ground measured crop characteristics (§3.2; table 4) and Landsat TM derived vegetation indices (§3.3; table 4) for 1998 data. Linear and nonlinear exponential

expressions (§3.7) were established for each crop or group of crops such as cereals (wheat and barley) and legumes (chickpea, lentil, vetch). Relationships that provide the best R^2 values are reported (see figure 3). Based on these well-understood relationships, biophysical and yield quantities are mapped for each farm in the TM data.

Agricultural crop types and other land use classes were mapped using unsupervised cluster ISOCCLASS algorithm in ERMapper™ software. Spectral classes were identified using ground data of crop types, GPS locations, crop growth stage and land cover percentages. Interpretation of data involved normalising for atmospheric effects, sensor degradation and solar illumination (see §3.4 to §3.7). Bispectral plots, multispectral plots and Normalized Difference Vegetation Index (NDVI) images were also used in interpretation.

4. Results

4.1. Mapping agricultural crops and land use classes of 1998 (near-real-time) image

Unsupervised classification was performed to generate initial 50 spectral classes in the study area using six non-thermal bands of the Landsat-5 TM image of 6 April 1998. Crops were identified based on ground data that included GPS referenced digital images, field maps of crop types, crop condition, canopy cover and crop growth stages (table 4). Wheat and barley could not be separated using any of the six non-thermal TM bands at 95% confidence level (see table 4) resulting in misclassifications (figure 2(a)). Similarly difficulties occurred in separating lentil and vetch/hay. NIR band TM4 could not differentiate between lentil and marginal lands, lentil and wheat, vetch and wheat. In contrast TM3 was able to differentiate these crops at 95% confidence limits (table 4). Overall, TM3 had the maximum number of 17 cases of discriminating between any two crops, followed by TM7 with 16 cases and TM5 with 15 (table 4). In an earlier study, Thenkabail *et al.* (2002) found a narrow band centred around 675 nm in red as the best band to estimate agricultural crop characteristics anywhere in the visible and NIR spectrum. Mid-infrared (MIR) based indices are known to perform equal to or better than NIR and red based indices in estimating biophysical variables such as biomass, LAI and plant height of crops (e.g. Shibayama and Akiyama 1989). Everitt *et al.* (1989) showed that the grass phytomass estimates were improved by MIR bands of Landsat TM (TM5 and TM7) when used as single wavelengths or as indices with NIR wavelengths. Tucker (1980) showed the leaf or biomass water sensitivity in 0.1550–0.1750 μm (TM5) and Thenkabail *et al.* (1994) demonstrated water stress detection capability in 0.2080–0.2350 μm (TM7).

However, groups of crops such as cereals (wheat and barley) can be discriminated from legumes (lentil, vetch/hay and chickpea). Cumin crop has distinct spectra from that of cereals or legumes due to its significantly lower biomass, LAI and late growing calendar (table 4). Apart from these, two classes of marginal lands (representing two biomass levels), trees/plantations, fallow farms and built-up/settlements were mapped. Roads/farm boundaries were manually digitized and overlaid for a total of nine crop and land use classes for 1998 TM data (figure 2(d)). The final nine classes were smoothed using a 3×3 majority filter to remove 'salt-and-pepper' noise. Seventy-two per cent of the total area was under agriculture. The nine classes (figure 2(d)) were mapped with an overall accuracy of 88% with $K_{\text{hat}} = 0.86\%$ (see table 6).

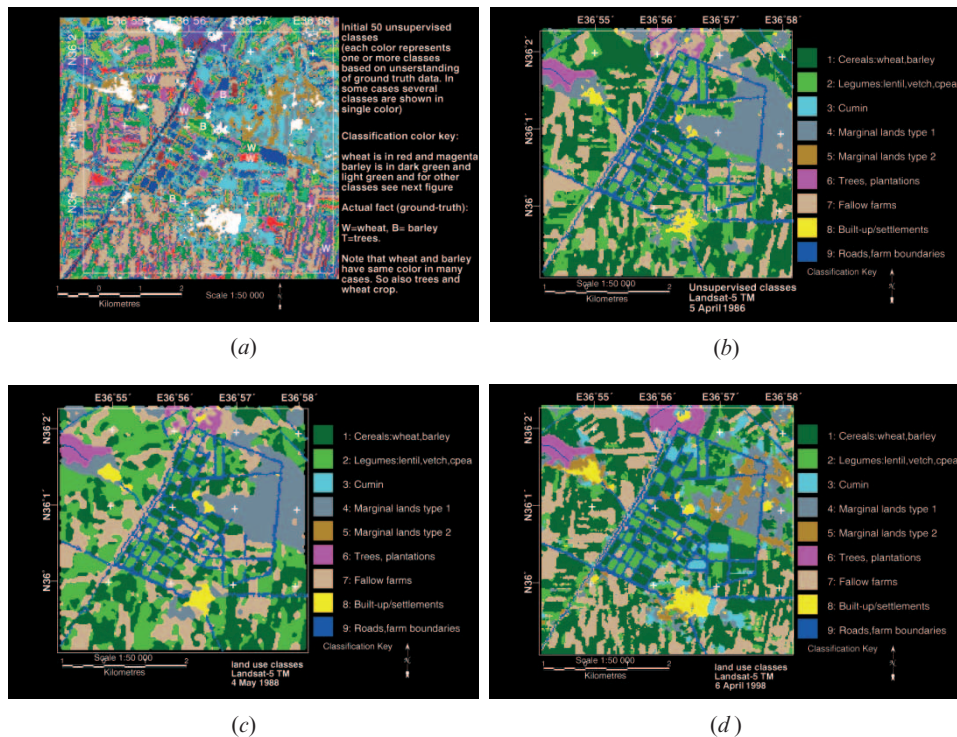


Figure 2. Agricultural land use classes. Initial 50 classes (a) of 6 April 1998 lead to final nine classes (d). The same nine classes were mapped for 5 April 1986 (b) and 4 May 1988 (c) using Landsat-5 TM data.

A similar procedure was used to map the nine agricultural and land cover classes using 1986 TM data (figure 2(b)) and 1988 TM data (figure 2(c)). Ground data of crop types were used to label unsupervised classes. The overall accuracy and K_{hat} values (not presented) varied between 0.81–0.85% for 1986 and 1988 images. The Cohen's Kappa or K_{hat} statistic allows for chance, and ranges from 0 in the case of the most confused classification to 1 in the case of the most accurate classification (Congalton 1991).

Crop and land use area statistics are provided for ICARDA research farms and the farmer-managed farms that surround them (table 5). This area was selected to test classification accuracies (see tables 6 and 7) since detailed data on crop types and crop calendars were available for these 3600 ha areas for all three years. Most of the cropped area was harvested or ready to harvest corresponding to 4 May 1988. So a direct comparison can only be made between the 5 April 1986 and 6 April 1998 images when crops were in late vegetative or critical growth phases. The overall cropped areas (classes 1, 2 and 3) have remained the same between 1986 and 1998. Cumin was not cultivated in 1986 or 1988. Some of the legume area during 1986 is taken by cumin in 1988. Cereal area has remained the same between 1986 and 1998 whereas fallow areas have decreased in 1998. The area of fallow is high during 1988 as a result of harvested farms. Significant rainfall events prior to 4 May 1988 resulted in marginal lands being greener with increasing volume of biomass and hence a large area under class 4 and no area under class 5.

Table 5(a). Agricultural and land use classes for the near-real-time (1998) and historical (1986 and 1988) images.

No.	Class	Colour	Area (ha) 6 April 1998	Area (ha) 5 April 1986	Area (ha) 4 May 1988	NDVI TM43 6 April 1998	NDVI TM43 5 April 1986	NDVI TM43 4 May 1988
1	Cereals: wheat, barley	dark green	1191.24	1170.94	797.061	0.69	0.55	0.52
2	Legume: lentil, vetch, chickpea	green	523.08	682.734	976.487	0.53	0.34	0.37
3	Cumin	cyan	180.45	0	0	0.07	–	–
4	Marginal lands 1: high LAI	yellow	320.13	259.77	475.085	0.57	–	–
5	Marginal lands 2: low LAI	orange	157.59	247.249	0	0.46	0.14	0.11
6	Trees, plantations	magenta	114.48	74.3209	100.44	0.41	0.29	0.31
7	Fallow farms, harvested areas	tan	683.1	784.641	851.33	0.05	0.01	–0.01
8	Built-up areas/settlements	sienna	110.43	68.0909	74.88	0.05	–0.03	–0.04
9	Roads, field boundaries	blue	319.41	312.164	324.65	0.12	0.06	0.08
	Total area		3599.91	3599.9098	3599.933			

Table 5(b). Biomass and LAI classes of agricultural crops for the near-real-time (1998) and historical (1986 and 1988) images.

No.	Class	Colour	LAI $\text{m}^2 \text{m}^{-2}$	Wet biomass kg m^{-2}	6 April 1998 Area (ha)	5 April 1986 Area (ha)	4 May 1988 Area (ha)
1	Marginal lands type 1: lowest LAI	grey		<0.40	188.64	491.49	475.085
2	Marginal lands type 2: medium LAI	yellow		0.40–0.75	204.12	0	0
3	Marginal lands type 3: high LAI	orange		>0.75	84.96	0	0
4	Legumes: lentil, vetch/hay, chickpea, cumin	aquamarine	<2.0	<1.0	261.35	183.19	408.1
5	Legumes: lentil, vetch/hay, chickpea, cumin	green-yellow	2.0–3.0	1.0–2.5	265.87	252.69	568.39
6	Legumes: lentil, vetch/hay, chickpea, cumin	green	3.0–4.0	2.5–3.75	108.63	232.54	0
7	Legumes: lentil, vetch/hay, chickpea, cumin	dark green	>4.0	>3.75	67.68	0	0
8	Cereals: wheat, barley	plum	<2.0	<2.0	232.57	232.475	396.2
9	Cereals: wheat, barley	tomato	2.0–3.5	2.0–3.3	358.88	394.429	400.862
10	Cereals: wheat, barley	red	3.50–5.0	3.3–4.6	513.91	512.855	0
11	Cereals: wheat, barley	magenta	>5.0	>4.6	85.88	0	0
12	Trees, plantations	blue violet			114.48	75.53	100.44
13	Fallow farms	wheat			683.1	841.71	851.33
14	Built-up/settlements	sienna			110.43	70.84	74.88
15	Roads, farm boundaries	blue			319.41	312.164	324.65
	Total area				3599.91	3599.913	3599.937

4.2. Accuracy of within and between field variability in mapping crops and land use

The accuracies were evaluated using detailed ground data and field based maps. The accuracy with which each crop is mapped is explained by the error matrix (table 6). The error matrix includes errors of omission (producer's error) and errors of commission (user's error). In this study, commission errors vary between 62–100% and omission errors between 71–100% (table 6). Maximum confusion in both within and between field variability occurred for the two marginal land classes and for cumin crop (table 6). Cumin had only 48% canopy cover resulting in highly significant reflectance contribution from the soil background, leading to significant confusion in cumin spectral values with those of marginal lands and fallow farms (table 6). Marginal lands, typically, constituted an inter-mix of wet and dry biomass, patches of barren areas, and had only 68% canopy cover (table 4). As a result accuracy of mapping these classes was lower relative to other classes (table 6).

4.3. Spectro-biophysical relationships

In order to map biomass and LAI using Landsat data, well-understood spectro-biophysical relationships are necessary. Legume (chickpea, lentil and vetch) and cumin NDVIs of TM data had linear relationship with: (a) LAI, explaining 78% of the variability (figure 3(a)); and (b) biomass, explaining 77% variability (figure 3(b)). Barley and wheat NDVIs had nonlinear exponential relationships with their biomass and LAI. The NDVI of the barley crop had less dynamic range (figure 3(c)) compared with wheat (figure 3(e) or (f)). The biomass of barley and marginal lands when pooled and related to NDVI explained 88% variability (figure 3(d)) in data. Least variability of 65% was explained for wheat LAI (figure 3(e)), followed by 67% for wheat biomass (figure 3(f)). In certain cases, relationships can be improved using indices from other TM wavebands, as discussed briefly in §4.7 and illustrated in figure 7. A detailed discussion of this falls outside the scope of this paper. Further discussions of the use of multiple wavebands of data in relationship with crop variables are given in detail by Lawrence and Ripple (1998) and Thenkabail *et al.* (1994).

Table 6. Accuracy assessment of crops and land use classes of the ICARDA study area using the Landsat-5 TM image of 6 April 1998 .

	1	2	3	4	5	6	7	8	9	Row total	User's accuracy (%)
1	683	13	0	0	0	0	2	0	0	698	98
2	13	407	0	25	5	0	6	2	0	458	89
3	1	0	178	8	2	0	17	6	0	212	84
4	1	2	23	164	62	0	4	2	5	263	62
5	1	7	10	30	241	0	13	29	7	338	71
6	0	0	0	0	0	254	0	0	0	254	100
7	2	8	19	4	6	0	626	0	4	669	94
8	0	0	2	0	2	0	10	141	9	164	86
9	0	2	5	0	0	0	3	3	112	125	90
Column total	701	439	237	231	318	254	681	183	137		
Producer's accuracy (%)	97	93	75	71	76	100	92	77	82		

Total number of pixels=3181; correctly classified pixels=2806, overall mapping accuracy 88%.

Classes: 1. cereals: wheat, barley; 2. legumes: lentil, vetch, chickpea; 3. cumin; 4. marginal lands type 1; 5. marginal lands type 2; 6. trees, plantations; 7. fallow farms; 8. built-up/settlements; 9. roads, farm boundaries.

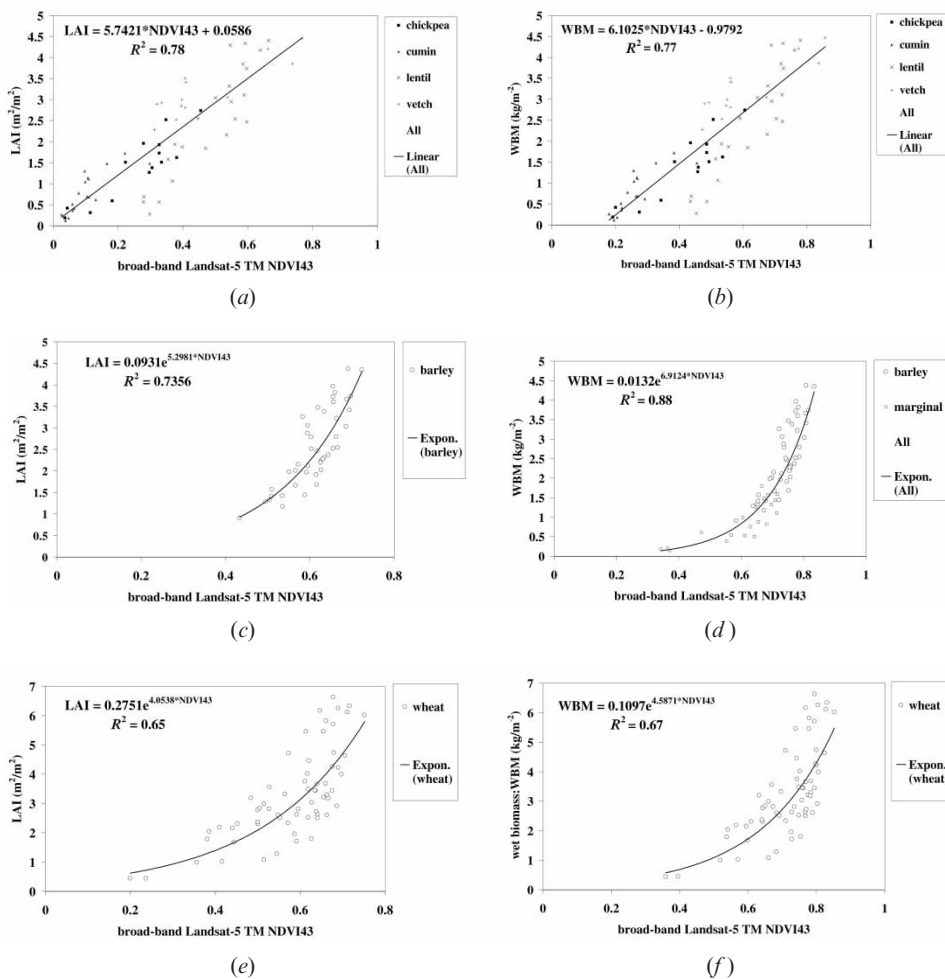


Figure 3. Relationships between broad-band Landsat-5 TM NDVI with biophysical variables. The TM NDVI are related to: (a) legumes (chickpea, lentil, vetch) and cumin LAI; (b) legumes and cumin WBM; (c) cereal barley LAI; (d) cereal barley and marginal lands WBM; (e) cereal wheat LAI; and (f) cereal wheat WBM.

The NDVI will have a certain degree of spectral mixing between crops (figure 4(a)). Thereby, across a range of crops (e.g. pooled data of all crops) NDVI explains a lesser degree of variability when related to relationships with quantitative biophysical characteristics. Significant improvements are possible by developing relationships with individual crops (e.g. figure 3(c)) and/or a group of crops (e.g. figure 3(d)).

Of the crops studied, wheat has the highest LAI and biomass (table 4). Vetch/hay and lentil have significantly higher LAI than barley. Vetch also has significantly higher biomass compared with barley. Yet barley has far greater absorption in TM3 [mean digital number (DN)= 20.7] when compared with TM3 DN values of 28.8 for vetch and 28.9 for lentil (table 4). This indicates that other factors such as the mesophyll structure unique to a plant, plant moisture, growth stage, growth condition, leaf structure, presence of nitrate in plant and a number of other factors

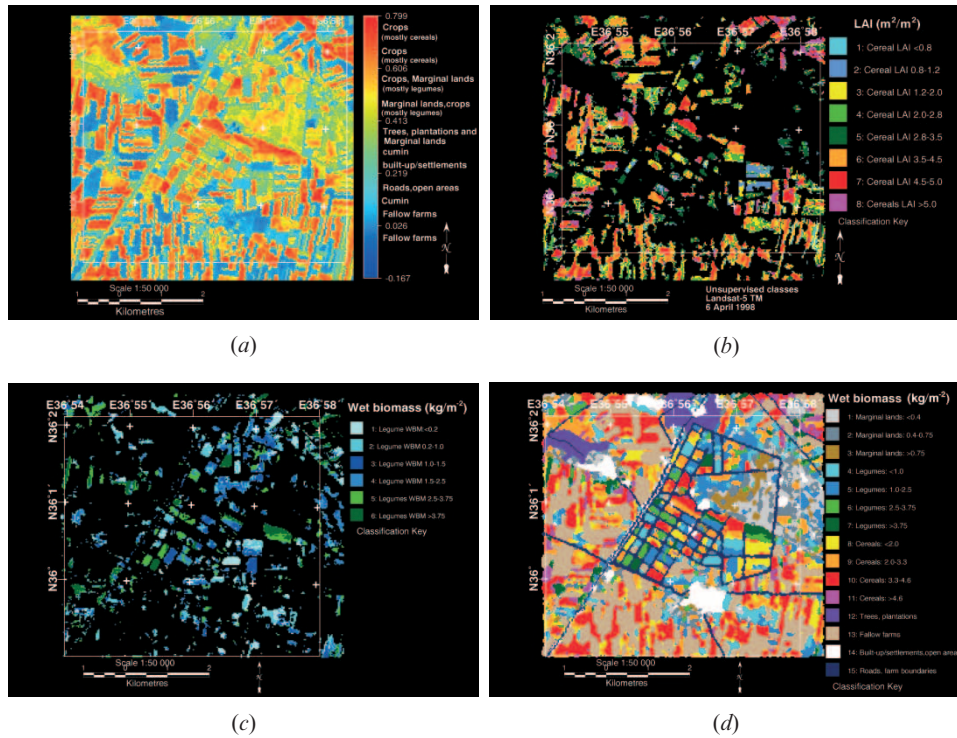


Figure 4. Steps in mapping LAI and WBM of agricultural crops, illustrated for the 6 April 1998 image: (a) NDVI vegetation gradient; (b) masking out non-agricultural areas to delineate LAI; (c) WBM; and (d) the resulting final biomass map.

play a part in the energy reflected. This fact suggests that crop types must be first discriminated before spectro-biophysical quantitative relationships are established. This requires more careful investigation.

4.4. Biomass and LAI variability within and between farms and pixels

Once the spectral index relationships with crop variables are well understood, these relationships are used to spatially map within and between farm variability in every farm and every pixel within a farm. The best spectro-biophysical relationships are established for individual crops or group of crops (figure 3). In order to spatially map these characteristics, we will need to either delineate each crop by their field boundaries or mask out their areas using land cover or crop-type classifications (see §4.1). Using classes of legumes alone, for example, mask out areas under legume crop (figure 4(c)). The six non-thermal bands from the image area of legumes are delineated from the rest of the image. This image file of legume crop was re-classified to 30 unsupervised classes, aggregated to six distinct information classes providing gradation of WBM levels (figure 4(c)) based on ground data, bispectral plots and spectro-biophysical relationships. The six WBM classes were further reduced to four in order to map the four classes with a higher degree of accuracy. Similarly, WBM levels of cereals (four classes) and marginal lands (three classes) are mapped. The remaining other classes were: trees or plantations, fallow farms, built-up area or settlements, and road networks. Biomass was not measured for other classes. The

above classes involving legumes, cereals and marginal lands are overlaid to obtain a contiguous mosaic of biomass map for the entire study area involving 11 classes. In addition four other classes (for which biomass was not available) were overlaid to obtain a total of 15 classes, 11 of which have biomass values (figure 4(d)).

A similar procedure was adopted for mapping LAI of legumes, cereals and marginal lands for the 1998 image (figure 5(c)). The exact cause of variability in biomass or LAI is often diagnosed based on field checks at a few points, leading farmers or farm managers to take appropriate management strategies (Moran *et al.* 1997).

4.5. Biomass and LAI from historical (archival) images or between seasons

For historical images (1986 and 1988) LAI and biomass were mapped with different strategy from that of near-real-time image described in §4.4. Unsupervised classification was performed on the historical images with 50 initial classes for the 1986 and 1988 data. Information classes were identified using crop type and crop calendar data. However, crop characteristics (e.g. biomass, LAI) data were not available for the historical images and hence were interpreted based on extrapolation from the relationships obtained for the near-real-time image of 1998 (see §4.3). The images of different years (1998, 1986 and 1988) had similar crops in the study area (§4.1) and were acquired when most crops were in similar growth stages. As a result

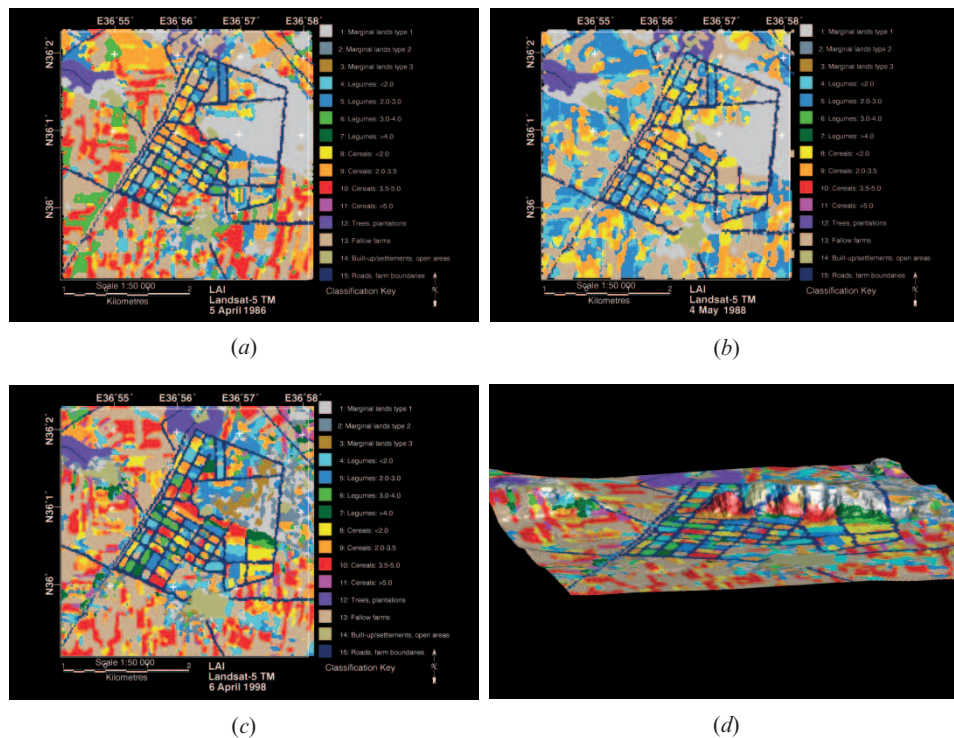


Figure 5. Mapping LAI using Landsat TM data. LAI maps of spring season crops at or near critical growth stages for: (a) 5 April 1986; (b) 4 May 1988; and (c) 6 April 1998. (d) The LAI of 1998 draped over 10m DEM data obtained from Russian TK-350 camera system.

the mean at-satellite reflectances of unsupervised classes were remarkably similar for the three years (figure 6). The trend of multispectral plots during three years remained consistent across images as seen for cereals (figure 6(a)), legumes (figure 6(b)), the two marginal land classes (figure 6(c)) and fallows (figure 6(d)). This implies that the spectro-biophysical relationships hold good across seasons. Factors such as differences in growth stages, growth conditions, changes in technology, differences in inputs will affect the dynamic range and magnitude of data from year to year. The growing conditions can vary substantially due to technological and management practices, and climatic variations. As a result we see minor changes in magnitudes of reflectances in 1986, 1988 and 1998 in figure 6.

Having the knowledge of across-season spectral behaviour of agricultural crop classes, we were able to map the same 15 classes for 1986, 1988 and 1998. These 15 classes include classes of biomass or LAI for cereals (wheat and barley) and legumes (vetch, chickpea and lentil), and classes of biomass or LAI for the marginal lands. The LAI mapped for 6 April 1985 (figure 5(a)) is compared with the LAI of 4 May 1988 (figure 5(b)) and LAI of 6 April 1998 (figure 5(c)).

Areas occupying different LAI and biomass levels for the three years are shown in table 5(b). The areas for LAI and biomass classes during 6 April 1998 (figure 5(c)) and 5 April 1986 (figure 5(a)) images were comparable (table 5(b)) with: (a) LAI < 5 and WBM < 4.6 kg m⁻² for cereals; and (b) LAI < 4 and WBM < 3.75 kg m⁻² for legumes. The area under the highest magnitude of LAI and biomass for cereals (LAI > 5, WBM > 4.6 kg m⁻²), legumes (LAI > 4, WBM > 3.75 kg m⁻²) and marginal lands (WBM > 0.75) were found for only 1998 (table 5(b); figure 5(c)), perhaps indicating technological and management advances in 1998. Only the low magnitudes of LAI and biomass were present in 4 May 1988 data (figure 5(b) and table 5(b)) as a result of advanced stages of senescing of crops.

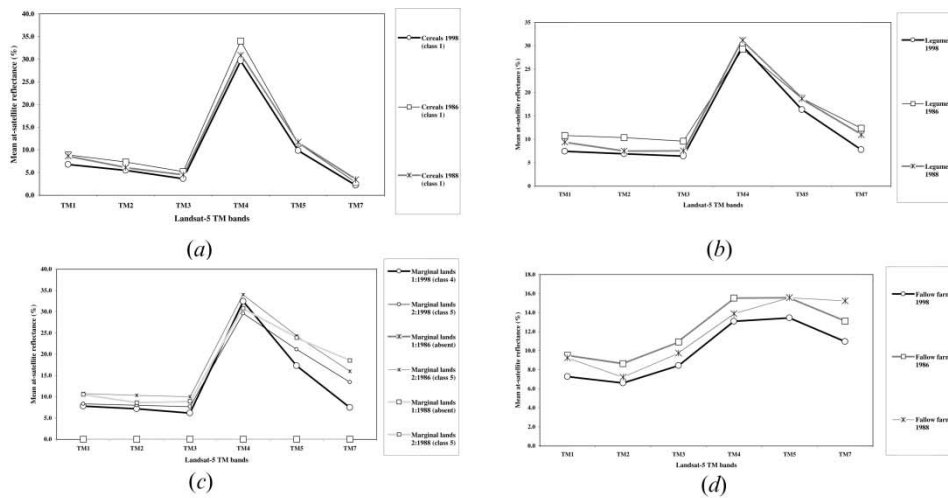


Figure 6. Reflectance of unsupervised classes in three years. At-satellite exoatmospheric mean reflectance characteristics of different land cover classes derived from unsupervised classification of three Landsat-5 TM images during late spring when crops are in critical or late vegetative or maturing growth stages.

4.6. Accuracy of within and between field variability in mapping biomass and LAI

The LAI and other classes of 1998 (figure 5(c)) were mapped at 81% overall accuracy (table 7) with $K_{\text{hat}} = 0.76$. The accuracy with which each crop is mapped is explained by the error matrix (table 7). Commission errors vary between 65–100% and omission errors between 56–100% (table 7). The results show that within crop variability (commission errors) is better explained by TM data than between field variability (omission errors). Maximum confusion in both within and between field variability occurred for the two marginal land classes (table 7) as a result of the inter-mix of wet and dry biomass, patches of barren areas, and significant soil background effects as a result of only 68% canopy cover (table 4). As a result accuracy of mapping these classes was least. The LAI map of 1998 (figure 5(c)) was overlaid on Russian TK-350 camera derived digital elevation model (DEM) data of 10m horizontal resolution to obtain a three-dimensional view (figure 5(d)). This shows marginal lands were mostly in higher elevations, making them more susceptible to moisture deficiency and as a result leading to a mix of dry and green patches, as well as open barren lands. Otherwise, errors occurred mostly as a result of confusion between two immediate categories such as between class 8 (cereals LAI < 2) and class 9 (cereals LAI 2–3.5). The overall accuracy and K_{hat} values for the 1986 and 1988 images varied between 0.71–0.77. Recent research has shown that hyperspectral bands provide significant additional information in estimates of biophysical characteristics (Blackburn 1998, Carter 1998, Thenkabail *et al.* 2000, 2002, Thenkabail 2002).

4.7. Field-by-field (and pixel-by-pixel) variability

Within and between field spatial variability are captured for every pixel in quantitative terms of biomass and LAI that have a well-established relationship with Landsat TM derived indices (figure 7). Spatial variability occurs due to various causes such as soil fertility or type variations, farm management (e.g. tillage and drainage) practices, non-uniform application of fertilisers, deficient or uneven rainfall distribution, uneven irrigation and topographic variations.

One representative farm in each of the six crops was selected for 1998 data (figure 7) to illustrate field-by-field (and pixel-by-pixel) variability in LAI and WBM. The lowest NDVIs across crops were mainly for the edge pixels of farm boundaries, which often have mixed pixel signatures of farm boundaries and farm. Near 100% canopy cover, critical growth stages, and high crop vigour ensured high levels of LAI and NDVI for barley (figure 7(a)) and wheat (figure 7(b)). The NDVI varied mostly between 0.50–0.75 (LAI 1.5 to >5) for barley. NDVI values below 0.5 were mostly edge or mixed pixels. For wheat, NDVI values mostly varied between 0.55–0.65 (LAI 2.41 to >5), with lower values for mixed or edge pixels. Both barley (figure 7(a)) and wheat (figure 7(b)) crops had portions of the field senescing (yellow) and portions in late vegetative (red). Pigmentation differences within these two fields due to varying growth conditions resulted in significant differences in within field variability for these crops. Earlier studies have shown the visible spectrum to be very sensitive to loss of chlorophyll, browning, ripening and senescing (Idso *et al.* 1980), carotenoid (Blackburn 1998) and soil background effects (Huete 1988).

Vetch had the highest leaf nitrogen content amongst all crops (table 4), was in late vegetative phase and had 88% canopy cover. These conditions resulted in high levels of NDVI and biomass. Vetch also has the highest plant moisture content (90%) of all crops. Hence, vetch was depicted using an index (NDVI53) with

Table 7. Accuracy assessment of leaf area index (LAI) map of the ICARDA study area using the Landsat-5 TM image of 6 April 1998.

	1	2	3	4	5	6	7	8	9	10	11	12	13	14	15	Row total	User's accuracy (%)
1	36	5	4	2	0	0	0	0	0	0	0	0	0	0	0	47	77
2	6	34	5	3	4	0	0	0	0	0	0	0	0	0	0	52	65
3	8	10	72	0	0	0	0	0	0	0	0	0	0	0	0	90	80
4	4	5	0	81	0	0	0	0	0	0	0	0	0	0	0	90	90
5	0	6	0	18	126	0	0	0	0	0	0	0	0	0	0	150	84
6	0	0	0	0	4	45	0	0	0	0	0	0	0	0	0	49	92
7	0	0	0	0	0	4	45	0	0	0	0	0	0	0	0	49	92
8	0	0	0	0	0	0	0	63	18	0	0	0	0	0	0	81	78
9	0	0	0	0	0	0	0	9	126	36	0	0	0	0	0	171	74
10	0	0	0	0	0	0	0	3	9	139	4	0	0	0	0	155	90
11	0	0	0	0	0	0	0	0	0	0	18	0	0	0	0	18	100
12	0	0	0	0	0	0	0	0	0	0	0	36	0	0	0	36	100
13	5	1	0	3	0	0	0	0	0	0	0	0	39	9	0	57	68
14	0	0	0	0	0	0	0	0	0	0	0	0	6	48	0	54	89
15	2	0	0	0	0	0	0	0	0	0	0	0	4	0	30	36	83
Column total	61	61	81	107	134	49	45	75	153	175	22	36	49	57	30	628	
Producer's accuracy (%)	59	56	89	76	94	92	100	84	82	79	82	100	80	84	100	779	81

Total number of pixels=779; correctly classified pixels=628; overall mapping accuracy=81%.

Classes: 1. marginal lands type 1; 2. marginal lands type 2; 3. marginal lands type 3; 4. legumes LAI= <2.0; 5. legumes LAI=2.0–3.0; 6. legumes LAI=3.0–4.0; 7. legumes LAI= >4.0; 8. cereals LAI= <2.0; 9. cereals LAI=2.0–3.5; 10. cereals LAI=3.5–5.0; 11. cereals LAI= >5.0; 12. trees, plantations; 13. fallow farms; 14. built-up/settlements; 15. roads, farm boundaries.

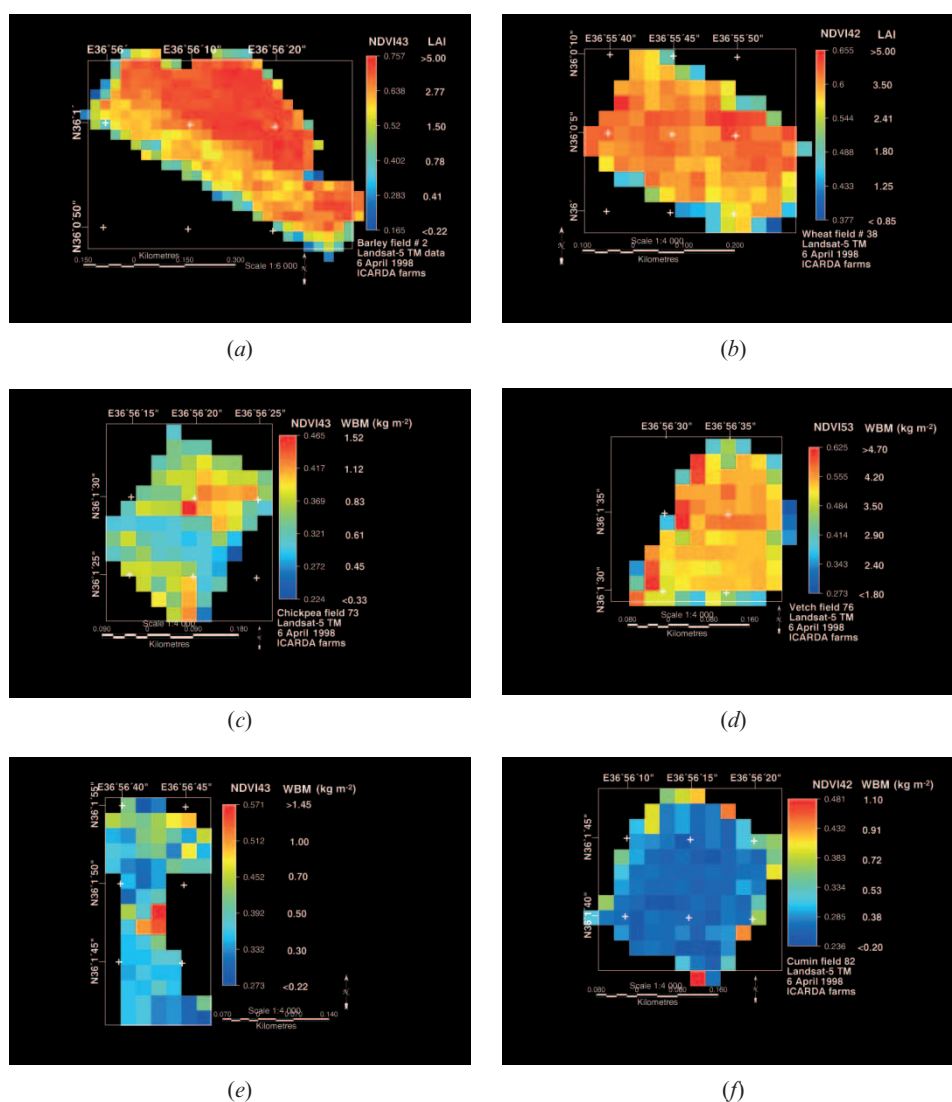


Figure 7. Within field spatial variability in LAI and WBM: (a) barley; (b) wheat; (c) chickpea; (d) vetch; (e) lentil; and (f) cumin. Variability of individual farms related to vegetation indices involving any two combinations of Landsat-5 TM bands at 2, 3, 4 and 5 for the 6 April 1998 image.

moisture sensitive TM5 band and red absorption band TM3 (figure 7(d)). Chickpea (figure 7(c)) and lentil (figure 7(e)) had significant soil background effects with about 70% canopy cover. As a result, within field variations were significant. For example, NDVI for a lentil field (figure 7(e)) varied between 0.27–0.57 (WBM <0.22 to <1.45). Flowering and significant soil background patches contributed to wide within field variations in chickpea biomass. Cumin was the only crop in early vegetative phase with 48% canopy cover. Soil background influences dominated this field (figure 7(f)) over any reflectance from vegetation, resulting in an NDVI value of about 0.25 (WBM <0.2 kg m⁻²). Soil background effects can be reduced using indices such as

Transformed Soil Adjusted Vegetation Index (TSAVI) (Elvidge and Chen 1995) especially for agricultural crops or homogeneous plant canopies (Rondeaux *et al.* 1996). The soil adjusted vegetation indices are more significant when agricultural crops on widely varying soils are studied (see, for example, Lawrence and Ripple 1998).

4.8. Temporal variability for a field

Temporal spatial variability was illustrated for a barley field (figure 8) using archival data of 1986 and 1988 and near-real-time data of 1998. In summer 1984, the field had no crop and hence the NDVI was very low, mostly below 0 (zero), for the entire farm (30 August 1984 image in figure 8) and is depicted here as a reference no crop condition. The NDVIs of different dates were normalised for atmospheric conditions, solar illumination, solar elevation and sensor degradation using calibration coefficients (table 3(a) and (b)). The NDVIs and LAIs during April–May of three spring dates for the barley crop in field number 2 were poor in 1988, moderate in 1986 and good in 1998 (figure 8). On similar lines, WBM and dry biomass (not illustrated) were poor during 1986, moderate during 1988 and good in 1998. A direct comparison of LAI can be made between 5 April 1986 and 6 April 1998. The NDVI (and LAI) of barley field number 2 was significantly higher during 1998 compared with 1986 (figure 8). Also the within field variability was considerably more during 1986. The LAI varied between 1.75 and > 5 during 1986 whereas it varied between 2.75 and > 5 during 1998. An overwhelming portion of the field had an NDVI > 0.7 (LAI > 4.5) during 1998 compared with only a small portion of the field with such high NDVI and LAI values during 1986 (figure 8). The variability may reflect one or more of the causes (e.g. crop vigour, crop condition, growth stages, stress

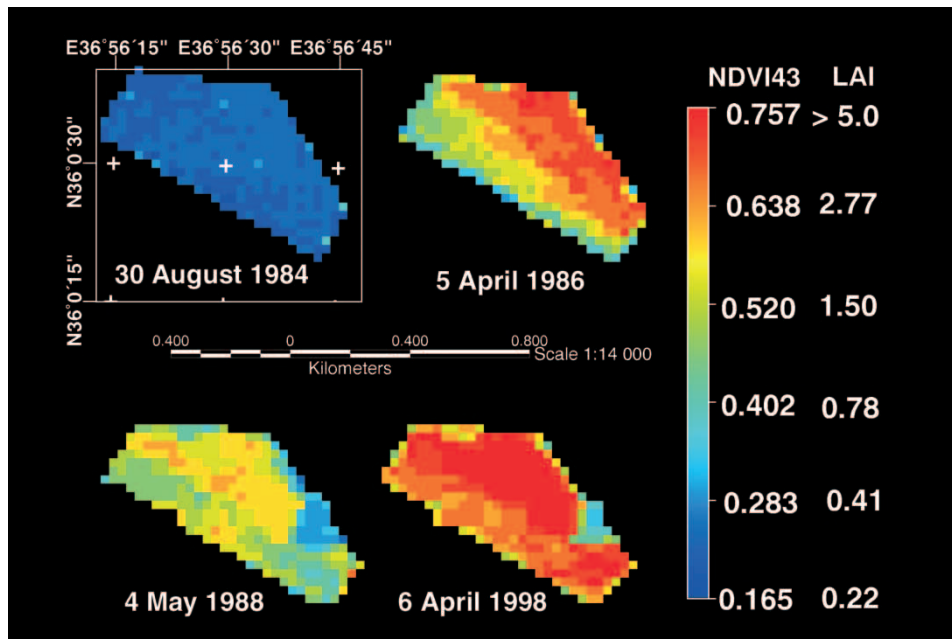


Figure 8. Temporal variations in LAI and NDVI for the 1986, 1988 and 1998 images compared with the base 1984 image, which had no crop.

conditions, variable application of pesticides and herbicides, soil characteristics) but was attributed to management factors (seed distribution, fertiliser distribution) and elevation differences (the field has significant within field slope variations). Mapping variability and quantifying it helps in targeting portions of the field that require better management practices or better applications of nutrients, and assessing losses incurred due to variability in the field. Quantitative relationships established using historical images add immense value to archival images. Also the consistent historical record of a farm is best seen using remotely sensed imagery over decades.

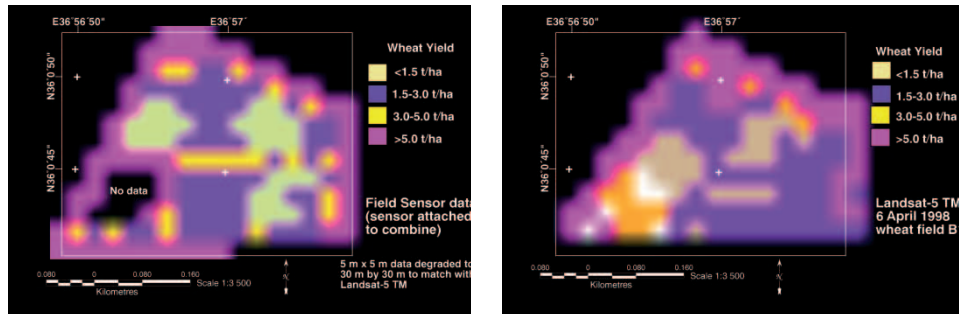
4.9. Yield variability

Crop yield measured using a combine-mounted sensor for field number 38 is illustrated (figure 9). Combine-mounted sensor provided wheat yield at every $5\text{ m} \times 5\text{ m}$. These data were disaggregated to $30\text{ m} \times 30\text{ m}$ (figure 9(a)) to correspond with Landsat TM pixel size. This results in a wheat yield map (figure 9(a)). Since pre-harvest crop yields are best predicted using images late in the crop-growing season (see Moran *et al.* 1997) the three images used in this study are ideal for predicting yield. The Landsat TM derived NDVIs of 1998 were related to after harvest yield (figure 9(d)). The TM NDVI variability for field number 38 is converted to yield variability (figure 9(b)) using NDVI vs after harvest yield (figure 9(d)). Thereby, a direct comparison of combine-mounted yield measurements (figure 9(a)) and Landsat TM derived yield measurements (figure 9(b)) was possible. Overall, there was a significant correlation between the combine measured and Landsat TM derived yield figures. These yield maps can be directly used for management of fertiliser application, water application, planting strategies, soil management, weeds, insects and diseases (Moran *et al.* 1997).

5. Conclusions

The results establish the capability of near-real-time and historical Landsat TM images to provide consistent within and between field spatial variability across seasons in biophysical characteristics (e.g. biomass, LAI) and yield that can be related to a crop model. This makes the decision-making approach feasible for precision farming applications. The utility of historical Landsat TM images that are available in data archive to provide quantitative biophysical characteristics of agricultural crops, based on modelling and understanding of spectro-biophysical relationships using real-time images, has been established. This adds great scientific and commercial value to archival TM data. The ability to look back in years at individual farms and pixels within the farms and to build land use histories and quantitative biophysical information levels for different time periods is of considerable significance in precision-farming applications.

Not all crop types could be well separated spectrally using TM data. However, crops when grouped into cereals (wheat and barley) and legumes (chickpea, lentil and vetch/hay) could be well discriminated using TM data. Nine agricultural and land cover classes were consistently mapped using a near-real-time image (1998) and two historical images (1986 and 1988) with high degrees of accuracy. Errors of commission (user's error) and errors of omission (producer's error) showing within and between field variability were (a) above 89% in mapping agricultural land cover classes, and (b) above 74% in mapping agricultural biophysical characteristics. The overall accuracies were (a) 88% ($K_{\text{hat}} = 0.86\%$) in mapping agricultural land cover classes, and (b) 81% ($K_{\text{hat}} = 0.76\%$) in mapping agricultural biophysical characteristics.

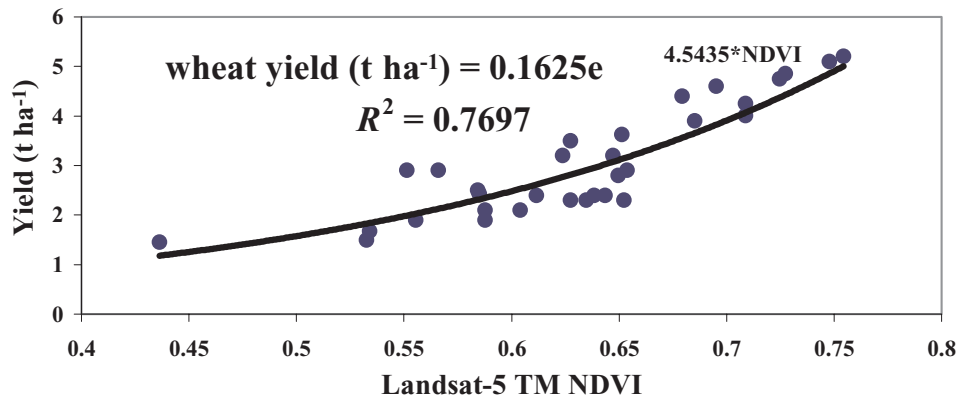


(a)

(b)



(c)



(d)

Figure 9. Yield variation in a wheat field measured using combine-mounted sensor (a) and Landsat-5 TM sensor (b). The field as seen during ground data collection is shown in (c). Relationship between actual after harvest yields with TM NDVI is shown in (d).

Acknowledgments

Financial support from the National Aeronautics and Space Administration (NASA) Earth Science Enterprise (grant number NAG5-3853) is gratefully acknowledged. Thanks to my colleagues at the Center for Earth Observation, Yale University: Dr Ronald B. Smith (Director), Dr Roland Geerken (Scientist) and Mr Laurent Bonneau (Laboratory Manager) for their support and discussions. Excellent fieldwork support was provided by the International Center for Agricultural Research

in the Dry Areas (ICARDA). Special thanks to: Dr Eddy de Pauw (Agroecologist), Mr A. F. Tarsha (Farm Manager), Dr Diekmann (Farm Director), Mr Afif Dakermanji (Research Manager) and Mr Pierre Hayak (Crop Scientist). Thanks to Professor Dr Adel El-Beltagy (Director General), Dr John H. Dodds (Assistant Director General, Research) and several others of ICARDA for all their support while collecting ground data used in this study.

References

- ANDERSON, G. L., HANSON, J. D., and HAAS, R. H., 1993, Evaluating Landsat Thematic Mapper derived vegetation indices for estimating above ground biomass on semiarid rangelands. *Remote Sensing of Environment*, **45**, 165–175.
- BARNES, E. M., MORAN, M. S., PINTER, P. J., JR, and CLARKE, T. R., 1996, Multispectral remote sensing and site-specific agriculture: examples of current technology and future possibilities. *Proceedings of the 3rd International Conference on Precision Agriculture, 23–26 June 1996, Minneapolis, MN, USA* (Madison, WI: American Society of Agronomy), p. 581.
- BLACKBURN, G. A., 1998, Spectral indices for estimating photosynthetic pigment concentrations: a test using senescent tree leaves. *International Journal of Remote Sensing*, **19**, 657–675.
- CARTER, G. A., 1998, Reflectance bands and indices for remote estimation of photosynthesis and stomatal conductance in pine canopies. *Remote Sensing of Environment*, **63**, 61–72.
- CHAVEZ, P. S., 1988, An improved dark-object subtraction technique for atmospheric scattering correction of multispectral data. *Remote Sensing of Environment*, **24**, 459–479.
- CHAVEZ, P. S., 1989, Radiometric calibration of Landsat thematic mapper multispectral images. *Photogrammetric Engineering and Remote Sensing*, **55**, 1285–1294.
- CONGALTON, R. G., 1991, A review of assessing the accuracy of classifications of remotely sensed data. *Remote Sensing of Environment*, **37**, 35–46.
- ELVIDGE, C. D., and CHEN, Z., 1995, Comparison of broad-band and narrow-band red and near-infrared vegetation indices. *Remote Sensing of Environment*, **54**, 38–48.
- ELVIDGE, C. D., YUAN, D., WEERACKOON, R. D., and LUNETTA, R. S., 1995, Relative radiometric normalization of Landsat multispectral scanner (MSS) data using an automatic scattergram controlled regression. *Photogrammetric Engineering and Remote Sensing*, **61**, 1255–1260.
- EVERITT, J. H., ESCOBAR, D. E., and RICHARDSON, A. J., 1989, Estimating grassland phytomass production with near-infrared and mid-infrared spectral variables. *Remote Sensing of Environment*, **30**, 257–261.
- FRITZ, L. W., 1996, The era of commercial earth observation satellites. *Photogrammetric Engineering and Remote Sensing*, **62**, 39–45.
- HUETE, A. R., 1988, A soil-adjusted vegetation index (SAVI). *Remote Sensing of Environment*, **25**, 295–309.
- IDSO, B., PINTER, P. J., JR, JACKSON, R. D., and REGINATO, R. J., 1980, Estimation of grain yields by remote sensing of crop senescence rates. *Remote Sensing of Environment*, **9**, 87–91.
- JOHANNSEN, C. J., BAUMGARDNER, M. F., WILLIS, P. R., and CARTER, P. G., 1998, Advances in remote sensing technologies and their potential impact on agriculture. *Proceedings of the First International Conference on Geospatial Information in Agriculture and Forestry, 1–3 June 1998, Lake Buena, FL, USA* (Lake Buena, FL: Veridian), p. 1348.
- JONES, D., and BARNES, E. M., 2000, Fuzzy composite programming to combine remote sensing and crop models for decision support in precision crop management. *Agricultural Systems*, **65**, 137–158.
- LAWRENCE, R. L., and RIPPLE, W. J., 1998, Comparisons among vegetation indices and bandwise regression in a highly disturbed, heterogeneous landscape: Mount St Helens, Washington. *Remote Sensing of Environment*, **64**, 91–102.
- MARKHAM, B. L., and BARKER, J. L., 1987, Radiometric properties of U.S. processed Landsat MSS data. *Remote Sensing of Environment*, **22**, 39–71.
- MILTON, E. J., 1994, Teaching atmospheric correction using a spreadsheet. *Photogrammetric Engineering and Remote Sensing*, **60**, 751–754.

- MORAN, S. M., MAAS, S. J., and PINTER, P. J., JR, 1995, Combining remote sensing and modeling for estimating surface evaporation and biomass production. *Remote Sensing Reviews*, **12**, 335–353.
- MORAN, M. S., INOUE, Y., and BARNES, E. M., 1997, Opportunities and limitations for image-based remote sensing in precision crop management. *Remote Sensing of Environment*, **61**, 319–346.
- NECKEL, H., and LABS, D., 1981, Improved data of solar spectral irradiance from 0.33 to 1.25 μm . *Solar Physics*, **74**, 231–240.
- NECKEL, H., and LABS, D., 1984, The solar radiation between 3300 and 12 500 Å. *Solar Physics*, **90**, 205–258.
- PRICE, J. C., 1987, Special issue on radiometric calibration of satellite data. *Remote Sensing of Environment*, **22**, 1–158.
- RONDEAUX, G., STEVEN, M., and BARET, F., 1996, Optimisation of soil-adjusted vegetation indices. *Remote Sensing of Environment*, **55**, 95–107.
- SHIBAYAMA, M., and AKIYAMA, T., 1989, Seasonal visible, near-infrared and mid-infrared spectra of rice canopies in relation to LAI and above-ground dry phytomass. *Remote Sensing of Environment*, **27**, 119–127.
- THENKABAIL, P. S., 2002, Optimal hyperspectral narrowbands for discriminating agricultural crops. *Remote Sensing Reviews*, **20**, 257–291.
- THENKABAIL, P. S., WARD, A. D., LYON, J. G., and MERRY, C. J., 1994, Thematic Mapper vegetation indices for determining soybean and corn crop parameters. *Photogrammetric Engineering and Remote Sensing*, **60**, 437–442.
- THENKABAIL, P. S., SMITH, R. B., and DE PAUW, E., 2000, Hyperspectral vegetation indices for determining agricultural crop characteristics. *Remote Sensing of Environment*, **71**, 158–182.
- THENKABAIL, P. S., SMITH, R. B., and DE PAUW, E., 2002, Evaluation of narrowband and broadband vegetation indices for determining optimal hyperspectral wavebands for agricultural crop characterization. *Photogrammetric Engineering and Remote Sensing*, **68**, 607–621.
- TUCKER, C. J., 1980, Remote sensing of leaf water content in the near infrared. *Remote Sensing of Environment*, **10**, 23–32.
- USERY, E. L., POCKNEE, S., and BOYDELL, B., 1995, Precision farming data management using Geographic Information Systems. *Photogrammetric Engineering and Remote Sensing*, **61**, 1383–1391.
- VAESEN, K., GILLIAMS, S., NACKAERTS, K., and COPPIN, P., 2001, Ground-measured spectral signatures as indicators of ground cover and leaf area index: the case of paddy rice. *Field Crops Research*, **69**, 13–25.